

Realization of the Heisenberg-Kitaev model in the honeycomb lattice iridates $A_2\text{IrO}_3$

Yogesh Singh,^{1,2} S. Mani,¹ and P. Gegenwart¹

¹*I. Physikalisches Institut, Georg-August-Universität Göttingen, D-37077, Göttingen, Germany*

²*Indian Institute of Science Education and Research Mohali, Sector 81, SAS Nagar, Manauli 140306, India*

(Dated: April 30, 2019)

Using thermodynamic measurements on the honeycomb lattice iridates $A_2\text{IrO}_3$ ($A = \text{Na}, \text{Li}$) we demonstrate that these materials are possible realizations of the Heisenberg-Kitaev model. Both materials are Mott insulators with effective spins $S = 1/2$ on a honeycomb lattice. The Curie Weiss temperature decreases from $\theta \approx -125$ K for Na_2IrO_3 to $\theta \approx -33$ K for Li_2IrO_3 . Surprisingly however, the antiferromagnetic ordering temperature for both materials is the same $T_N \approx 15$ K. This counter-intuitive behavior directly mimics the recent predictions of the finite temperature Heisenberg-Kitaev model on a honeycomb lattice. Our results also indicate that the Li_2IrO_3 system is close ($0.6 \leq \alpha \leq 0.7$) to the Kitaev limit ($\alpha \geq 0.8$) and that application of pressure might tune it to the spin-liquid state expected in the Kitaev limit of the model.

Introduction: Recently the Kitaev model of spins $S = 1/2$ on a honeycomb lattice has attracted a lot of attention because it is a relatively simple spin model involving only nearest neighbor interactions and yet it shows several exotic states of matter.¹ The ground state is a gapless spin-liquid with emergent Majorana excitations, or a gapped topologically ordered state (the Z_2 spin-liquid) with Abelian anyonic excitations depending on the model parameters.¹ Yet another exotic phase of the Kitaev model is obtained when the spin-liquid is gapped out by applying a magnetic field perpendicular to the honeycomb plane.^{1,2} This phase is also a gapped, topologically ordered phase, but one with non-abelian quasiparticle (Majorana fermions) statistics.^{2,3} Among systems predicted to support Majorana fermions are exotic fractional quantum Hall systems⁴ and heterostructures of topological insulators, semi-metals, or semiconductors with conventional s -wave superconductors.⁵ Realizations of the Kitaev model and its extensions would also be avenues to look for these elusive quasiparticles.

The Kitaev model is thus relevant to such diverse areas as quantum computation^{1,6} and strongly correlated condensed matter systems^{7,8} among others and search for realizations of this and related models is of fundamental importance.

In looking for experimental realizations of the Kitaev model one must not only look for systems with $S = 1/2$ on the honeycomb lattice. In addition one also needs to look at how to introduce anisotropic exchange interactions required in the model. Superconducting circuits⁹ and optical lattices¹⁰ have been proposed as possible ways of realizing the Kitaev model. In solid state materials, Mott insulating transition metal oxides with strong spin-orbit coupling have been suggested as possible candidates.^{7,11}

The layered iridate Na_2IrO_3 has effective $S = 1/2$ Ir^{4+} moments on a honeycomb lattice.¹² The strong spin-orbit coupling in this 5d transition metal system is likely to lead to orbital dependent anisotropic in-plane exchange. However, one needs to worry about the possibility of other interactions like the isotropic Heisenberg interactions being present in addition to the Kitaev like inter-

actions. Such a Heisenberg-Kitaev (HK) model has been studied recently and found to have an interesting phase diagram depending on the relative strength of the two terms. The HK Hamiltonian can be written as¹¹

$$H_{\text{HK}} = (1 - \alpha) \sum_{ij} \vec{\sigma}_i \cdot \vec{\sigma}_j - 2\alpha \sum_{\gamma} \sigma_i^{\gamma} \cdot \sigma_j^{\gamma} \quad (1)$$

where the σ_i are the Pauli matrices for the effective $S = 1/2$ and $\gamma = x, y, z$ labels the three different links for each spin of the honeycomb lattice. The first part in Eq.(1) is the isotropic Heisenberg term while the second term is the anisotropic Kitaev term.¹¹ The Heisenberg exchange is antiferromagnetic, while the anisotropic Kitaev exchange is ferromagnetic. Varying the relative coupling strength $0 \leq \alpha \leq 1$, the model interpolates from the simple Heisenberg model with a Néel ground state for $\alpha = 0$ to the Kitaev model for $\alpha = 1$, which even for ferromagnetic interactions is highly frustrated and exhibits a gapless spin-liquid ground state.¹ As the coupling α is varied, three magnetic phases were found in zero temperature calculations¹¹ and have been found to persist in calculations at finite temperatures too.¹³ The three phases are a simple Néel antiferromagnet for $0 \leq \alpha \leq 0.4$, a stripy antiferromagnet for $0.4 \leq \alpha \leq 0.8$, and a spin-liquid state for $0.8 \leq \alpha \leq 1$.^{11,13}

Even though the $A_2\text{IrO}_3$ materials have been suggested as possible avenues to look for Kitaev like and HK like physics,^{7,11,13} there is very limited experimental data available for the $A_2\text{IrO}_3$ systems. We have earlier shown that single crystal Na_2IrO_3 is a Mott insulator which undergoes antiferromagnetic ordering below $T_N = 15$ K although the polycrystalline samples showed glassy behavior.¹² There are two conflicting reports on the magnetic properties of Li_2IrO_3 .^{14,15} The first report suggested paramagnetic behavior between $T = 5$ K and 300 K without any sign of magnetic order¹⁴ while the second report showed an anomaly in the magnetic susceptibility below $T = 10$ K which was also accompanied by a hysteresis between zero-field-cooled and field-cooled data suggesting glassy behavior.¹⁵ No heat capacity data

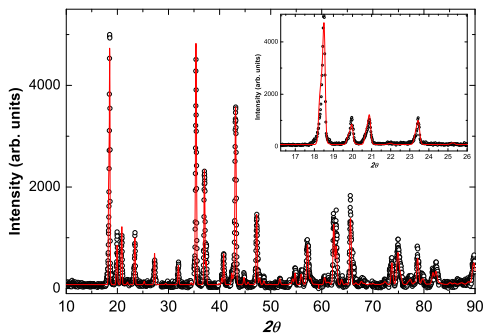


FIG. 1: Rietveld refinement of the X-ray diffraction data of polycrystalline Li_2IrO_3 . The closed symbols represent the observed data, the solid lines represent the fitted pattern. Regions where small ($\leq 10\%$) peaks of LiCl appeared have been excluded in the fits. The inset shows an expanded view of the data at low angles.

is available for Li_2IrO_3 . Recent resonant x-ray scattering measurements on single crystal Na_2IrO_3 shows that the magnetic order is most likely a stripy kind¹⁶ suggesting that this system lies in the $0.4 \leq \alpha \leq 0.8$ region of the HK model.

Herein we report magnetic and heat capacity measurements on high quality polycrystalline samples of $A_2\text{IrO}_3$ ($A = \text{Na}, \text{Li}$). Magnetic measurements show local moment behavior with effective spin $S = 1/2$ moments. Both magnetic and heat capacity measurements show sharp anomalies at $T_N = 15$ K for both materials indicating bulk antiferromagnetic ordering. The evolution of the Curie-Weiss temperature scale θ and the ordering scale T_N directly mimic recent predictions¹³ for the finite temperature Heisenberg-Kitaev model indicating that the $A_2\text{IrO}_3$ ($A = \text{Na}, \text{Li}$) materials are the first realizations of this model in real solid-state materials.

Experimental: Polycrystalline samples of $A_2\text{IrO}_3$ ($A = \text{Na}, \text{Li}$) and Li_2SnO_3 were synthesized by solid state synthesis. High purity starting materials $A_2\text{CO}_3$ ($A = \text{Na}, \text{Li}$) (99.995% Alfa Aesar) and Ir metal powder ($\geq 99.95\%$ Alfa Aesar) or SnO_2 (99.995% Alfa Aesar) were mixed in the ratio 1.05 : 1 and placed in an alumina crucible with a lid and given heat treatments between 750 °C and 950 °C in steps of 50 °C with intermediate grindings and pelletizing after each step. The Li_2SnO_3 sample was given a further heat treatment at 1000 °C. In an attempt to grow single crystals the Li_2IrO_3 sample was dissolved in excess LiCl flux at 850 °C for 6 hrs and then cooled to 590 °C at 3 °C/hr. After washing majority of the LiCl flux with de-ionized water we obtained a fine black powder which turned out to be highly ordered Li_2IrO_3 polycrystalline samples. This powder was pelletized and sintered at 900 °C for 48 hrs to get a hard pellet for resistivity and heat capacity measurements.

The resistivity (not shown) for sintered Li_2IrO_3 is insulating with a room temperature value $\approx 35 \Omega \text{ cm}$ and an activation gap ≈ 700 K.

Structure: Powder x-ray diffraction (XRD) scans of

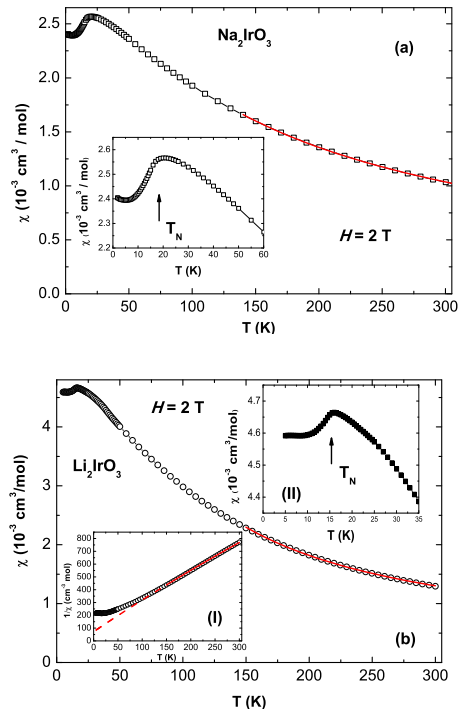


FIG. 2: (Color online) (a) Magnetic susceptibility χ versus temperature T for Na_2IrO_3 . The fit by the Curie-Weiss (CW) expression $\chi = \chi_0 + C/(T - \theta)$ is shown as the curve through the data. The inset shows the anomaly at the antiferromagnetic ordering. (b) χ versus T for Li_2IrO_3 . The solid curve through the data is a fit by the CW expression. The inset (I) shows the $1/\chi(T)$ data for Li_2IrO_3 . The solid curve through the data is a fit by the CW expression and the dashed curve is an extrapolation of the fit to lower T . The inset (II) shows the anomaly at the onset temperature of antiferromagnetic ordering.

polycrystalline $A_2\text{IrO}_3$ ($A = \text{Na}, \text{Li}$) and Li_2SnO_3 were found to be single phase and could be indexed to the monoclinic $C2/c$ (No. 15) structure. Rietveld refinements,¹⁷ of the x-ray patterns gave the unit cell parameters $a = 5.4187(2) \text{ \AA}$, $b = 9.3689(3) \text{ \AA}$, $c = 10.7731(5) \text{ \AA}$ and $\beta = 99.598(18)^\circ$ for Na_2IrO_3 and $a = 5.1678(4) \text{ \AA}$, $b = 8.9347(7) \text{ \AA}$, $c = 9.7825(4) \text{ \AA}$ and $\beta = 99.998(14)^\circ$ for Li_2IrO_3 . A representative XRD scan for Li_2IrO_3 obtained by LiCl flux method is shown in Fig.1 along with the Rietveld refinement shown as the curve through the data. Regions where small peaks of LiCl appeared have been excluded in the fits. Figure 1 inset shows the XRD data and Rietveld refinement at low angles on an expanded scale. The highly ordered nature of the sample can be seen from the separation of the lines between $2\theta = 19$ and 22° which in a disordered sample would appear merged together and would also show a highly anisotropic shape with a tail extending to the higher angle side of the peak.^{18,19}

Magnetic Susceptibility: The magnetic susceptibility $\chi = M/H$ versus T data for Na_2IrO_3 are shown in

Fig. 2(a). The $\chi(T)$ data between $T = 150$ K and 300 K were fit by the Curie-Weiss expression $\chi = \chi_0 + \frac{C}{T-\theta}$ with χ_0 , C , and θ as fitting parameters. The fit, shown in Fig. 2(a) as the solid curve through the data gave the values $\chi_0 = 3.6(4) \times 10^{-5} \text{ cm}^3/\text{mol}$, $C = 0.40(2) \text{ cm}^3 \text{ K/mol}$, and $\theta = -125(6) \text{ K}$, respectively. The above value of C corresponds to an effective moment of $\mu_{\text{eff}} = 1.79(2) \mu_B$ assuming a g -factor $g = 2$. This value of μ_{eff} is close to the value $1.74 \mu_B$ expected for spin = 1/2 moments. The inset in Fig. 2(a) shows the $\chi(T)$ data at low temperatures to highlight the anomaly seen at the onset of the antiferromagnetic transition below $T_N = 15$ K. The values of C , μ_{eff} , and T_N obtained above for polycrystalline Na_2IrO_3 match very well with the values we observed earlier for single crystals of Na_2IrO_3 indicating the high quality of the polycrystalline samples used in this study.¹²

The $\chi(T)$ data for Li_2IrO_3 are shown in Fig. 2(b). Li_2IrO_3 shows local-moment behavior and the $\chi(T)$ data above $T = 150$ K were fit by the Curie-Weiss expression $\chi = \chi_0 + \frac{C}{T-\theta}$. The fit is shown as the solid curve through the $\chi(T)$ data in Fig. 2(b). The data were also analyzed in another way. The $1/\chi(T)$ data between $T = 150$ K and $T = 300$ K were also fit by the above Curie-Weiss expression. The fit is shown in Fig. 2(b) inset (I) as the solid curve through the data and the dashed curve is the extrapolation of the fit to lower T . The two fits for Li_2IrO_3 above gave the average values $\chi_0 = 8.1(7) \times 10^{-5} \text{ cm}^3/\text{mol}$, $C = 0.42(3) \text{ cm}^3 \text{ K/mol}$, and $\theta = -33(3) \text{ K}$, respectively. The above value of C corresponds to an effective moment of $\mu_{\text{eff}} = 1.83(5) \mu_B$ which is close to the value $1.74 \mu_B$ expected for spin = 1/2 moments. This behavior along with the insulating resistivity above indicates that Li_2IrO_3 like Na_2IrO_3 is a Mott insulator. The value of the Weiss temperature $\theta = -33(3) \text{ K}$ for Li_2IrO_3 suggests that the effective antiferromagnetic exchange interactions have weakened compared to the Na_2IrO_3 system. Surprisingly however, the $\chi(T)$ data for Li_2IrO_3 also show an anomaly at 15 K as seen in Fig. 2(b) inset II. This suggests that an antiferromagnetic transition still occurs at $T_N = 15$ K for Li_2IrO_3 . This is supported by our heat capacity results presented below.

Heat Capacity: Figure 3(a) shows the heat capacity divided by temperature C/T versus temperature T data for Na_2IrO_3 . The anomaly at $T_N = 15$ K confirms bulk magnetic ordering in our polycrystalline Na_2IrO_3 samples again indicating their high quality. Figure 3(b) shows the C/T versus T data for Li_2IrO_3 and the non-magnetic analog Li_2SnO_3 . The C/T data for Li_2IrO_3 shows a clear anomaly at $T_N = 15$ K confirming the bulk nature of the antiferromagnetic ordering observed in the χ data in Fig. 2(b) inset II above. A small bump is also observed around $T = 5$ K in the $C(T)$ for Li_2IrO_3 . This most likely arises due to a small amount ($\leq 5\%$) of disorder in the sample.¹⁹ To obtain the magnetic contribution to the total $C(T)$ for Li_2IrO_3 , the $C(T)$ of Li_2SnO_3 is used as an approximate estimation of the lattice contribution to

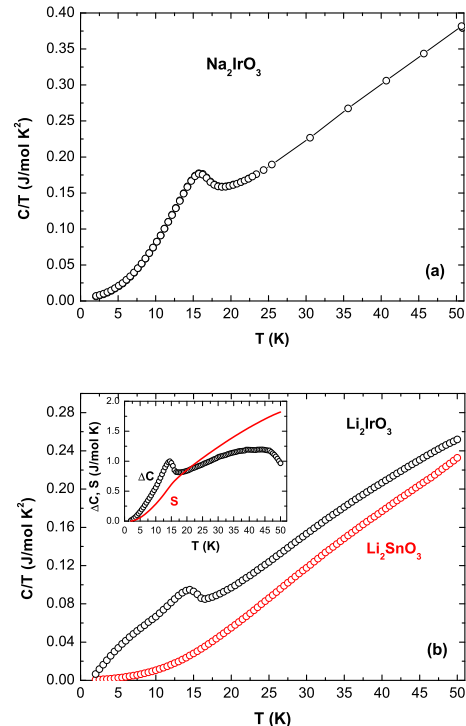


FIG. 3: (Color online) (a) The heat capacity divided by temperature C/T versus T data between $T = 1.8$ K and 40 K for single crystals of Na_2IrO_3 and the heat capacity of Na_2SnO_3 as the lattice contribution C_{lattice}/T versus T . The inset shows the C/T versus T data in $H = 0$ and 7 T applied magnetic field. (b) The difference heat capacity ΔC and difference entropy ΔS versus T data between $T = 1.8$ K and 40 K.

the heat capacity of Li_2IrO_3 . Figure 3(b) inset shows the difference heat capacity $\Delta C(T)$ obtained by subtracting the $C(T)$ data of Li_2SnO_3 from the $C(T)$ data of Li_2IrO_3 . A lambda-like anomaly at $T_N = 15$ K is more clearly visible in the $\Delta C(T)$ data for Li_2IrO_3 . A slight depression of T_N in an applied magnetic field of $H = 9$ T was observed (not shown) which points to the antiferromagnetic nature of the magnetic ordering in Li_2IrO_3 . The difference entropy $S(T)$ obtained by integrating the $\Delta C/T$ versus T data is also shown in Fig. 3(b) inset. Just above T_N the entropy is only about $15\% \ln 2$. A reduced entropy at the transition was also observed earlier for single crystalline Na_2IrO_3 .¹²

Relevance of our results to the Heisenberg-Kitaev model: From our previous¹² and current study of structural, magnetic, and thermal properties we have established that the $A_2\text{IrO}_3$ ($A = \text{Na}, \text{Li}$) materials contain a honeycomb lattice of strongly spin-orbit coupled localized effective spin $S = 1/2$ moments, making these materials possible avenues to look for Kitaev like physics as has also been pointed out before.^{7,11} These materials have effective antiferromagnetic exchange interactions and long-range antiferromagnetic ordering at low temper-

atures. If the exchange interactions were purely Kitaev like they would have been ferromagnetic and we would have obtained a positive Weiss temperature θ and additionally the ground state would have been a spin-liquid. Therefore, the magnetic properties of these materials are not governed entirely by Kitaev physics alone.

If on the other hand the exchange interactions were entirely Heisenberg like, then these materials would have shown a simple Néel type antiferromagnetic ordering. However, recent resonant x-ray scattering measurements on single crystalline Na_2IrO_3 have established that the magnetic order is not a simple Néel antiferromagnet but is rather of a stripy antiferromagnetic kind.¹⁶ Such a stripy AFM state has been predicted for the Heisenberg-Kitaev model when the parameter α in the model lies in the range $0.4 \leq \alpha \leq 0.8$.^{11,13} Given the similarities of the magnetic anomalies in the $\chi(T)$ and $C(T)$ data for both Na_2IrO_3 and Li_2IrO_3 it is most likely that Li_2IrO_3 also shows a similar stripy antiferromagnetic structure. Thus there are strong indications that the A_2IrO_3 materials lie in the region $0.4 \leq \alpha \leq 0.8$ of the Heisenberg-Kitaev model. Calculations of the finite temperature Heisenberg-Kitaev model predict that if the system stays in the region where $0.4 \leq \alpha \leq 0.8$ then θ monotonically decreases with increasing α .¹³ Remarkably however, it is also predicted that the magnetic ordering temperature stays unchanged between $0.4 \leq \alpha \leq 0.7$ and only starts dropping significantly as one approaches the Kitaev limit beyond $\alpha \geq 0.8$ where long range order is replaced by a spin-liquid state as the ground state.¹³ The reduction of the Weiss temperature scale on increasing α is natural since the Heisenberg term comes with an antiferromagnetic sign and the Kitaev term comes with a ferromagnetic sign. This reduction in the Weiss temperature scale is indeed observed for our systems where θ decreases from ≈ -125 K to ≈ -33 K on going from Na_2IrO_3 to the Li_2IrO_3 system. We can get a lower-limit estimate of the proximity of the Li_2IrO_3 system to the Kitaev limit of $\alpha \geq 0.8$ by assuming that Na_2IrO_3 sits at the lower edge $\alpha = 0.4$ of the region in which the stripy antiferromagnetism is observed. We can then use the theoretical predictions of the variation of the Weiss temperature versus α [Ref. 13] and our experimental estimates of θ for

Na_2IrO_3 and Li_2IrO_3 to obtain $\alpha \approx 0.6$ as a lower limit for Li_2IrO_3 . Thus, Li_2IrO_3 lies very close to the Kitaev limit $\alpha \geq 0.8$.

In going from the Na to the Li system the a, b lattice parameters are reduced by $\approx 4.5\%$ while the c parameter is reduced by $\approx 10\%$. Thus, substituting Na by Li is equivalent to preferentially applying chemical pressure along the c axis (\perp to the honeycomb planes). This leads to a decrease of the c -axis distortion of the IrO_6 octahedra which enhances the parameters $\eta_{1,2}$ leading to an increased Kitaev coupling.¹¹ This is consistent with the value of $\alpha \geq 0.6$ for Li_2IrO_3 which puts it closer to the Kitaev limit.

In addition to the above reduction of the Weiss scale, the antiferromagnetic ordering temperature $T_N \approx 15$ K is the same for both Na_2IrO_3 and Li_2IrO_3 despite a factor of ≈ 5 reduction of θ . This counter-intuitive result is again in direct agreement with the above theoretical predictions of the finite temperature Heisenberg-Kitaev model.¹³ The above independence of T_N on θ for $0.4 \leq \alpha \leq 0.7$ and the factor of 8 reduction of T_N compared to θ for the Na system, are issues that will need to be addressed in future experimental and theoretical work.

In summary, our results provide the strongest support yet that the A_2IrO_3 materials are the first realization of the Heisenberg-Kitaev model in real solid-state materials. From the above comparison of experiment and theory it is also clear that Li_2IrO_3 lies close to the $\alpha \geq 0.8$ Kitaev limit. The application of c -axis pressure to the A_2IrO_3 materials can push them closer to the Kitaev limit and the Li_2IrO_3 system should be easier to tune given that it most likely lies close to $\alpha = 0.8$.

Acknowledgments

Discussions with S. Trebst are gratefully acknowledged. YS acknowledges support from Alexander von Humboldt foundation. SM acknowledges support from the Erasmus Mundus Eurindia Project.

¹ A. Kitaev, Ann. Phys. (N.Y.) 321, 2 (2006).

² H. Jiang, Z. Gu, X. Qi, and S. Trebst, arXiv:1101.1145 (2011).

³ A. Stern, Nature 464, 187 (2010).

⁴ M. Storni and R. H. Morf, Phys. Rev. B 83, 195306 (2011).

⁵ Y. Oreg, G. Refael, F. von Oppen, Phys. Rev. Lett. 105, 177002 (2010).

⁶ C. Zhang et al, Proc. Natl. Acad. Sci. USA 104, 18415 (2007); S. Dusuel, K. P. Schmidt, and J. Vidal, Phys. Rev. Lett. 100, 177204 (2008).

⁷ G. Jackeli and G. Khaliullin, Phys. Rev. Lett. 102, 017205 (2009).

⁸ K. S. Tikhonov, M. V. Feigel'man, and A. Yu. Kitaev, Phys. Rev. Lett. 106, 067203 (2011).

⁹ J. Q. You, X.-F. Shi, X. Hu, and F. Nori, Phys. Rev. B 81, 014505 (2010).

¹⁰ L.-M. Duan, E. Demler, and M. D. Lukin, Phys. Rev. Lett. 91, 090402 (2003).

¹¹ J. Chaloupka, G. Jackeli, and G. Khaliullin, Phys. Rev. Lett. 105, 027204 (2010).

¹² Y. Singh and P. Gegenwart, Phys. Rev. B 82, 064412 (2010).

¹³ J. Reuther, R. Thomale, and S. Trebst, arXiv:1105.2005, (2011).

- ¹⁴ I. Felner and I. M. Bradari, *Physica B* **311**, 195 (2002).
- ¹⁵ H. Kobayashi, M. Tabuchi, M Shikano, H Kageyamaa, and R. Kanno, *J. Mater. Chem.* **13**, 957 (2003).
- ¹⁶ X. Liu, T. Berlijn, W.-G. Yin, W. Ku, A. Tsvetik, Y. J. Kim, H. Gretarsson, Y. Singh, P. Gegenwart, and J. P. Hill, arXiv:1104.4046, (2011).
- ¹⁷ A. C. Larson and R. B. Von Dreele, "General Structure Analysis System (GSAS)", Los Alamos National Laboratory Report LAUR 86-748 (2000). B. H. Toby, *J. Appl. Cryst.* **34**, 210 (2001).
- ¹⁸ M. J. O'Malley, H. Verweij, P. M. Woodward, *J. Solid State Chem.* **181**, 1803 (2008).; M. J. O'Malley Ph.D. thesis, Ohio State Univ. (2009).
- ¹⁹ S. Manni *et al.* unpublished.